Overcoming redox reactions at perovskite/nickel oxide interfaces to boost voltages in perovskite solar cells

Caleb C. Boyd,[1,2,3] R. Clayton Shallcross,[4] Taylor Moot,[2] Ross Kerner,[2] Luca Bertoluzzi,[1] Arthur Onno,[5] Shalinee Kavadiya,[5] Cullen Chosy,[6] Eli J. Wolf,[2,3,7] Jérémie Werner,[2,3] James A. Raiford,[6] Camila de Paula,[6] Axel F. Palmstrom,[2] Zhengshan J. Yu,[5] Joseph J. Berry,[2] Stacey F. Bent,[6] Zachary C. Holman,[5] Joseph M. Luther,[2] Erin L. Ratcliff,[8] Neal R. Armstrong,[4*] Michael D. McGehee[2,3,9,10*]

Affiliations

[1]Department of Materials Science and Engineering, Stanford University, Stanford, CA 94305, USA.
[2]National Renewable Energy Laboratory, Golden, CO 80401, USA.
[3]Department of Chemical and Biological Engineering, University of Colorado, Boulder, CO 80309, USA.
[4]Department of Chemistry and Biochemistry, University of Arizona, Tucson, AZ 85721, USA,
[5]School of Electrical, Computer, and Energy Engineering, Arizona State University, Tempe, AZ 85281, USA.
[6]Department of Chemical Engineering, Stanford University, Stanford, CA 94305, USA.
[7]Department of Applied Physics, Stanford University, Stanford, CA 94305, USA.
[8]Department of Materials Science and Engineering, University of Arizona, Tucson, AZ 85721, USA
[9]Materials Science and Engineering, University of Colorado, Boulder, CO 80309, USA.
[10]Lead Contact
[*]Correspondence to: michael.mcgehee@colorado.edu and nra@email.arizona.edu

Summary

Nickel oxide (NiO_x) hole transport layers (HTLs) are desirable contacts for perovskite solar cells because they are low-cost, stable, and readily scalable; however, they result in lower open-circuit voltages (V_{OC}s) as compared to organic HTLs. Here, we characterize and mitigate electron transfer-proton transfer reactions between NiO_x HTLs and the precursors of mixed cation perovskite active layers. Using XPS/UPS characterization, we identify that the near surface region of NiO_x thin films exhibits under-coordinated $Ni^{\geq 3+}$ metal cation sites that are redox active and act both as Brønsted proton acceptors and Lewis electron acceptors, deprotonating cationic amines and oxidizing iodide species, driving the formation of hole-extraction barriers consisting of A-site deficient or $PbI_{2-x}Br_x$-rich perovskites at the perovskite/NiO_x interface. Titrating reactive $Ni^{\geq 3+}$ surface states with excess formamidinium salts during perovskite active layer deposition yielded an increase in V_{OC} values to 1.15 V and power conversion efficiencies of ~20%. We posit that this may be a more general finding for all semi-transparent metal oxide contacts that can act as both Brønsted acid/base and Lewis acid/base reactants toward perovskite precursors, an observation that has also been made recently for TiO_2 and SnO_2 interlayers and contacts.

Introduction

Metal halide perovskite solar cells have largely fulfilled their potential of combining III-V-like optoelectronic properties with low-cost, solution-processing deposition techniques, achieving single-junction power conversion efficiencies (PCEs) >25%.[1,2] Remaining challenges include scaling the technology from square-millimeter laboratory devices to square-meter modules with good long-term stability, all while maintaining low-cost targets necessary in the highly competitive silicon-dominated solar market.[3] A nickel oxide (NiO_x) thin film deposited over a semi-transparent electrode such as indium-tin oxide (ITO) is a highly desirable wide bandgap hole harvesting contact for perovskite solar cells and organic solar cells because it is low-cost, stable, and readily scalable.[4–8] NiO_x hole transport layers (HTL) can be pre-fabricated as nanoparticles and coated in thin films[9–16] or formed directly on the substrate using a variety of processing routes including sol-gel, [5,17–20] spray coating,[21] atomic layer deposition (ALD),[22,23] and sputtering;[8,24–28] many of which enable large area coating, roll-to-roll coating, low temperature processing, and processing on textured or rough surfaces, which is particularly relevant for monolithic tandem devices.[22,27,28] Perovskite solar cells with NiO_x HTLs have delivered some of the best reported stability results under a variety of stressors, including the 85 °C/85% relative humidity damp heat test, temperature cycling from -40 °C to 85 °C, and extended operational stability at elevated illumination and temperature.[23,27,29–33] However, perovskite solar cells made with NiO_x HTLs typically result in lower open-circuit voltages (V_{OC}) compared to ultra-thin, undoped organic hole transport layers, which are more expensive and present problems for both scalability and stability. Enhancing the V_{OC} and increasing efficiency of NiO_x-based devices will directly result in a decreased module cost ($/W).

While many reports describe treatments and processing techniques to improve voltages and device efficiencies of perovskite solar cells on nickel oxide,[9,11,13,15–18,34–36] there remains little consensus on the fundamental limitations and, hence, pathways to improve photo-voltages in perovskite solar cells with NiO_x HTLs. Band alignment of the NiO_x/perovskite interface is often cited as a driving factor in device performance. However, this conflicts with some reports that the HTL ionization potential (IP) or work function (Φ) is not critical to V_{OC} in perovskite-based photovoltaics.[37,38] Further, the IP of NiO_x thin films (~5.2 eV) is similar to those of polymeric materials such as poly(4-butylphenyl-diphenyl-amine) (poly-TPD) or poly(triaryl amine) (PTAA) that deliver much higher V_{OC}s.[39,40] A second hypothesis is that interfacial

electronic defects or traps increase surface recombination in NiO_x over its organic counterparts, but this conflicts with reports that surface recombination velocities of perovskite films on NiO_x and PTAA are equivalent,[41] a finding that we verify in this manuscript using external radiative efficiency measurements (ERE).

In other energy conversion technologies, including electrocatalysts and photoelectrochemical systems, NiO_x readily participates in surface-assisted reactions with an electrolyte or adjacent material, and the nature of these reactions depends on the chemical and electronic structure of the NiO_x. We hypothesize that similar interfacial chemistry between perovskite precursors and the oxide surface can also explain the sub-optimal photovoltages in NiO_x-based perovskites. That such a chemically reactive surface exists for NiO_x is supported by several recent demonstrations of surface treatments, resulting in V_{OC} values of ~1.1V and PCEs above 18%.[9,17,18,34,35] Examples include using extrinsic doping of the NiO_x HTL with Li, Cu, or Cs[11,13,15,16,36] or surface treatments with K^+ or Na^+ species,[9,17] butylamine,[34] or ionic liquids.[35] However, there is no consensus on the types of chemical defects that are being "passivated" or on the mechanism that limits voltage in devices using NiO_x HTLs without these treatments.

Here, we identify a surface-assisted electron transfer-proton transfer (ET-PT) mechanism at the NiOx/perovskite interface leading to barriers for hole harvesting and device V_{OC} loss. Specifically, under-coordinated metal cation sites ($Ni^{\geq 3+}$) act both as a Lewis acid/oxidant towards dissociated lead halide precursors (i.e. I^-) and as a Brønsted base (proton-acceptor) with protonated amine precursors. The collective ET-PT mechanism, demonstrated by spectroscopic analysis, explains the formation of A-site deficient – and therefore $PbI_{2-x}Br_x$-rich – perovskite at the perovskite/NiO_x interface. This defective perovskite region both increases recombination at the interface and acts as a hole extraction barrier, either by limiting hole mobility to the HTL or by acting as an energetic barrier, resulting in device V_{OC} loss. We show that the reaction is self-limiting based on the number of $Ni^{\geq 3+}$ sites, similar to interfacial reactions previously demonstrated on n-type oxide layers such as ZnO,[42,43] TiO_2,[44,45] and SnO_2.[46]

We demonstrate the elimination of the extraction barrier via a simple, easily scaled approach: titration of surface oxide proton-acceptor sites by incorporating 1-5 mol% excess A-site cation to the perovskite precursor solution. This amount is sufficient to counteract the loss of organic cation, preventing formation of a $PbI_{2-x}Br_x$ layer at the interface, ultimately leading to a V_{OC} increase >200 mV. We demonstrate that this mechanism applies to all forms of NiO_x,

including thin films created from sol-gel precursors, nanoparticles, atomic layer deposition (ALD), and radio frequency (RF) sputtering, and is generalizable across multiple perovskite active layers, including state-of-the-art single junction and tandem relevant compositions. A p-i-n perovskite solar cell with 19.7% PCE at maximum power point (MPP) and V_{OC} up to 1.15 V is achieved. Devices maintain >90% of their initial performance after 2000 hours of thermal stability testing at 85 °C or >80% of their initial performance after 400 hours of accelerated operational stability testing under illumination and 55 °C in nitrogen. Our results extend the generality of acid/base-coupled oxidation-reduction reactions as the driving force for interface equilibration at metal oxide/perovskite interfaces, suggesting that metal halide perovskites have similar reactions with many types of metal oxide layers.

Results

Voltage Deficit and $PbI_{2-x}Br_x$ Formation in Perovskite Active Layers on NiO_x

We focus our discussion on $Cs_{0.25}FA_{0.75}Pb(Br_{0.2}I_{0.8})_3$ (CsFA, FA is formamidinium) perovskite active layers used for highly efficient perovskite/silicon tandem solar cells,[47,48] and we extrapolate our mechanistic findings to the more commonly used $Cs_{0.05}MA_{0.16}FA_{0.79}Pb_{1.03}(Br_{0.16}I_{0.86})_3$ (triple cation, MAFACs, MA is methylammonium) perovskite composition.[49,50] These compositions have demonstrated the typical large V_{OC} losses when NiO_x HTLs are used in p-i-n solar cells.[48] Unless stated otherwise, all results were obtained for NiO_x layers sputtered from a stoichiometric NiO target in pure Ar at room temperature without any post-treatments, which we label throughout the manuscript "as-deposited" or "as-dep" (see **Methods**). The as-deposited NiO_x surface was found to be highly reproducible, as shown by X-ray and ultraviolet photoelectron spectroscopy (XPS and UPS) measurements on samples from various deposition runs over months (**Figures S1**) with an average work function (Φ) of 4.1 eV and an onset in ionization potential (IP) at 5.2 eV (**Figure S2**).

Figure 1B and **Table 1** summarize characteristic p-i-n photovoltaic device performance metrics for CsFA on various HTLs: poly-TPD, PTAA, and sputtered NiO_x. The metrics shown are a representative set of ~80 devices made in our lab over the past year. We observed a significantly diminished V_{OC} (~200 mV lower) for NiO_x relative to the organic-based HTLs despite similar electronic structure, with the IP at ~5.2 eV for PTAA, poly-TPD, and NiO_x.[39,40,48] Similar morphologies were observed via scanning electron microscopy for the perovskite on both PTAA and NiO_x, suggesting that the issue was not related to bulk formation of the perovskite on

different substrates (**Figure S3**). We then turned to X-ray diffraction (XRD) to examine differences in the perovskite active layer, such as the formation of $PbI_{2-x}Br_x$, when deposited on the organic versus inorganic HTLs.[31] As shown in **Figures 1C & 1D**, CsFA formed on NiO_x had more $PbI_{2-x}Br_x$ and smaller lattice parameters by about 0.01Å than when formed on PTAA. We note that there is a small amount of $PbI_{2-x}Br_x$ formation for PTAA as well, similar to many other reports of high-performing perovskite compositions.[49,51,52] We speculate that there is no detrimental effect of $PbI_{2-x}Br_x$ for the PTAA layer because it is dispersed throughout the film, while the additional $PbI_{2-x}Br_x$ present in the perovskite on NiO_x is concentrated at the interface between the perovskite and the NiO_x, creating an extraction barrier to holes as we show below.

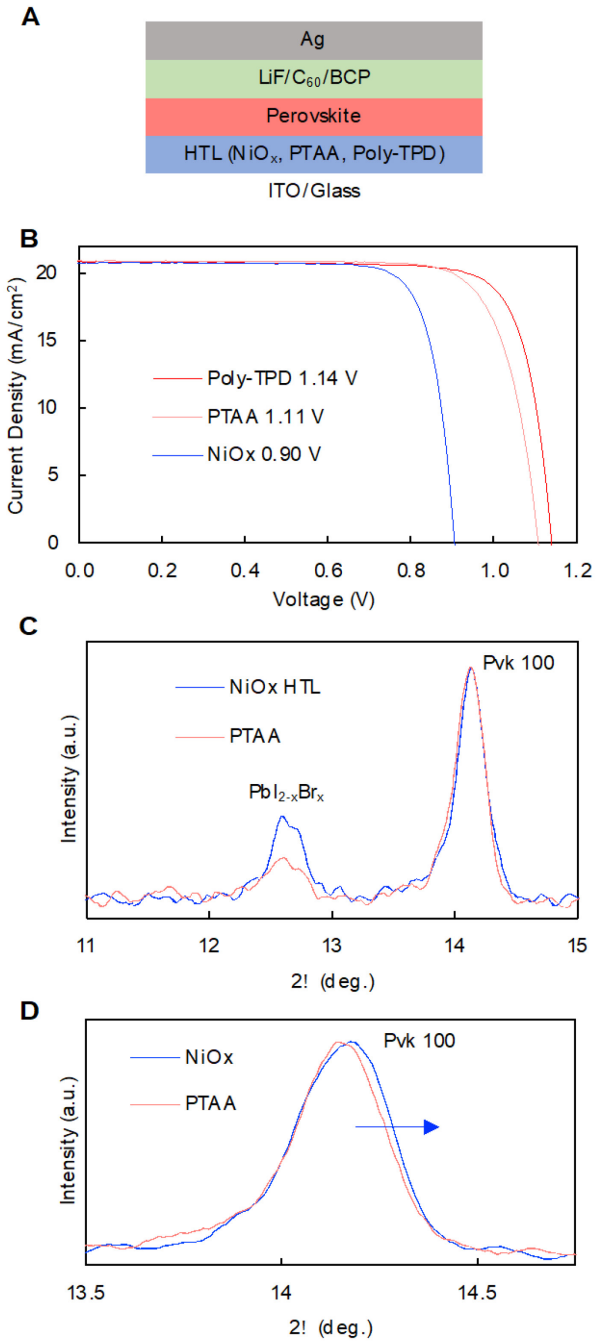

Figure 1 Voltage Deficit and $PbI_{2-x}Br_x$ Formation in Perovskite Active Layers on NiO_x: (A) Schematic of the p-i-n solar cell structure used in this study. (B) Current-voltage curves of p-i-n $Cs_{0.25}FA_{0.75}Pb(Br_{0.2}I_{0.8})_3$ solar cells with NiO_x, PTAA, or poly-TPD hole transport layers (HTLs), showing characteristic loss in voltage of solar cells deposited on NiO_x. (C), (D) X-ray diffraction peaks of $Cs_{0.25}FA_{0.75}Pb(Br_{0.2}I_{0.8})_3$ perovskite on NiO_x and PTAA

showing an increase in $PbI_{2-x}Br_x$ (C) and a decrease in lattice parameter (D, blue arrow denotes perovskite peak shifts to higher 2θ angles) on perovskite deposited on NiO_x.

Table 1: Averages and standard deviations of current-voltage parameters including open-circuit voltage (V_{OC}), short-circuit current (J_{SC}), fill factor (FF), and power conversion efficiency (η) for *n* $Cs_{0.25}FA_{0.75}Pb(Br_{0.2}I_{0.8})_3$ solar cells on various hole transport layers (HTLs). The ionization potential (IP) with respect to vacuum is also shown.

HTL	IP (eV)	*n*	V_{OC} *(V)*	J_{SC} *(mA/cm²)*	FF (%)	η (%)
Poly-TPD	5.2[40]	29	1.12 ± 0.02	20.42 ± 0.20	80.8 ± 4.4	18.55 ± 1.28
PTAA	5.2[39]	26	1.11 ± 0.02	20.53 ± 2.66	74.0 ± 6.2	16.63 ± 0.28
NiO_x	5.2	28	0.89 ± 0.02	20.72 ± 0.44	79.2 ± 4.3	14.57 ± 0.97

Organo-iodide Precursors React with NiO_x

The observed higher amounts of crystallized $PbI_{2-x}Br_x$ on NiO_x suggests the presence of a chemical reaction between NiO_x and the perovskite. To test this hypothesis, we used a UV-ozone (UVO) surface treatment of the NiO_x as a model case to increase the number of defects in the NiO_x film and more clearly identify reactions with the perovskite precursor.[7,8,53,54] We note that UVO treatment was detrimental to device efficiencies due to increased absorption in the NiO_x and increased reactivity with the perovskite, therefore UVO treatment was not used in devices. Upon the UVO treatment we observed a physical darkening of the NiO_x film due to an increase in sub-bandgap absorption but no change in the primary absorption onset (**Figure 2A and Figure S4**). This coincided with an increase in Φ to ~4.8 eV and in IP to ~5.4 eV observed via ultraviolet photoelectron spectroscopy (**Figure S2**) and suggests the formation of a number of mid-gap states. This change in absorption has been reported to be due to an increase in $Ni^{\geq 3+}$ sites,[53] consistent with our XPS results described below. We used photoelectron spectroscopy (**Figure S2**) to estimate the valence band distributions and optical spectroscopy (**Figure S4**) to estimate the conduction band distributions culminating in a estimated density of states (DOS) (**Figure 2B**). The UVO treatment of NiO_x introduces a number of under-coordinated cations, resulting in a decrease in the occupied DOS at the valence band (increased number of holes). Finally, we observed an increase in the amount of $PbI_{2-x}Br_x$ when the perovskite film was deposited on UVO-treated NiO_x in comparison to as-deposited NiO_x films (**Figure S4**). This suggests that the increase in these $Ni^{\geq 3+}$ sites is directly tied to the formation of $PbI_{2-x}Br_x$, which agrees with prior identification of $Ni^{\geq 3+}$ sites as reactive catalytic sites for oxidation, including

oxygen evolution, ammonia oxidation, and the conversion of I^- to I_3, and surface-assisted electron transfer and/or proton transfer mechanisms (either PT-ET or ET-PT).[55–57]

Qualitative assessment of the UVO-treated NiO_x/perovskite precursor reactions is summarized in **Figures 2A,D, and E**, which was divided into two experiments to deconvolute the reaction chemistries of the halide (I, Br, or Cl) (**Figure 2D**) and cation (FA, MA, Cs, or Pb) (**Figure 2E**). In **Figure 2D, E**, experiments were run in anhydrous acetonitrile (ACN) solvent, whereby judicious exclusion of H_2O ensured there were no adventitious protons – outside of those associated with the organic cations – available for reaction with NiO_x. FAI and MAI clearly reacted with the nickel oxide, visibly bleaching the film (**Figure 2A**) and reducing the sub-bandgap defect density as shown by a bleach of the sub-bandgap absorption (**Figure 2D**). In contrast, the FABr and MABr did not react with the NiO_x film to an extent that was detectible by eye or UV-Vis spectroscopy. Treating NiO_x films with ACN alone had no effect (**Figure 2A, Figure S4)**. Similar results were obtained for precursors dissolved in dimethylformamide (DMF), a more popular solvent for perovskite precursor inks (**Figure S5**), as well as when dissolved in water (**Figure S6**). No NiO_x bleaching was observed with inorganic halide precursors (PbI_2 and CsI) in the absence of a proton source (ACN solvent or organic cation) (**Figure 2A&E**) but bleaching was observed in water (**Figure S6**). Thus, $Ni^{\geq 3+}$ sites are capable of oxidizing iodide only when there is a proton donor present, but neither bromide nor chloride due to their much higher oxidation potentials.[58] This is consistent with our hypothesis of active $Ni^{\geq 3+}$ sites in all NiO_x contacts acting as a Brønsted base – deprotonating the precursor amine – and as a Lewis acid – oxidizing I^-, as shown in the schematic in **Figure 2C**. Complementary data for the as-deposited NiO_x layers are provided in **Figure S7**, where we observed similar trends, although to a lesser extent than with UVO films, indicating that our analysis of reactions of the perovskite with UVO NiO_x can be extrapolated to the as-deposited NiO_x layers as well (we examine this quantitatively with XPS results below). The data on UVO treated NiO_x thin films, which clearly have the greatest surface density of reactive defects, demonstrates that processing can significantly influence the surface reactivities in these HTLs.

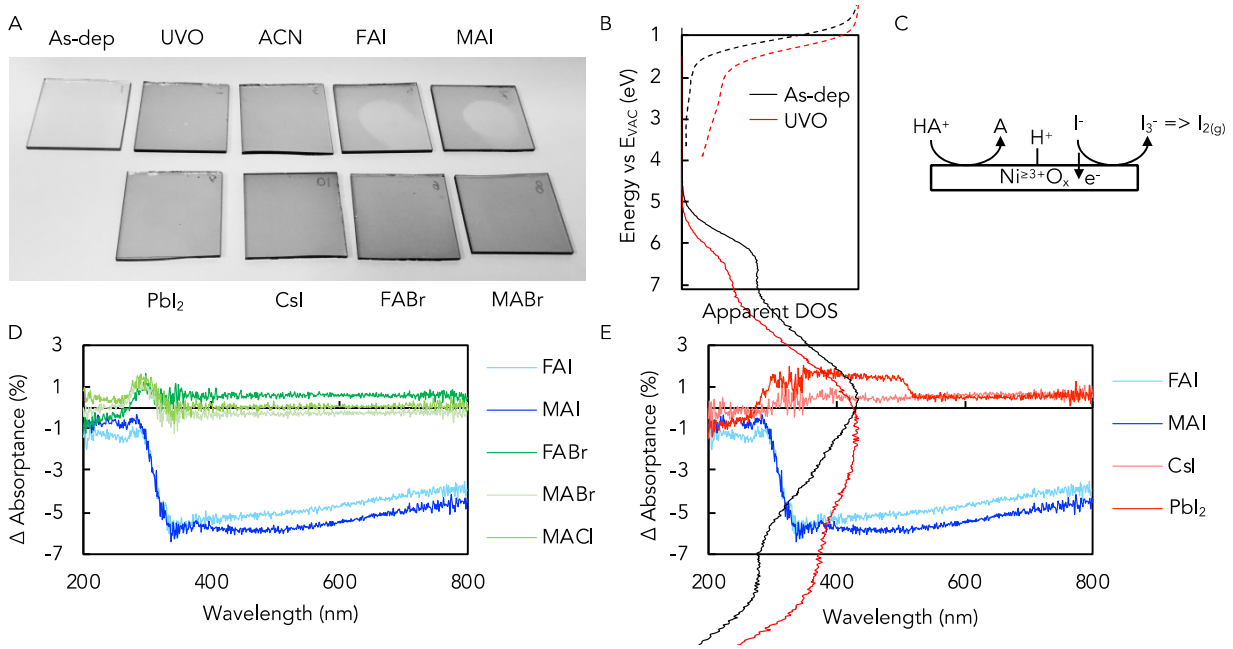

Figure 2 Organo-iodide Precursors React with NiO_x: (A) Photograph of NiO_x films as-deposited (As-dep) and treated with UV-ozone (UVO) and various perovskite precursors (FAI, FABr, MAI, MABr, PbI_2, CsI) dissolved in acetonitrile (ACN). (B) Estimated density of states (DOS) for NiO_x as-deposited (As-dep, black) and UV-ozone treated (UVO, red). (C) Schematic depicting the electron transfer-proton transfer mechanism at $Ni^{\geq 3+}O_x$ surface states, which both deprotonate cation amines such as formamidinium and methylammonium, here designated as HA^+, and oxidize iodide, forming I_3^- which is in equilibrium with $I_{2(g)}$. (D) Change in absorptance of UVO-treated NiO_x films after a 1 minute treatment with a drop of 0.1 M solution in ACN of (D) MAI (dark blue), FAI (light blue), MABr (light green), MACl (medium green), or FABr (dark green); and (E) the same data is shown for MAI (dark blue), FAI (light blue), CsI (light red), and PbI_2 (dark red). All treatments are followed by an ACN wash.

To provide further mechanistic insight of reaction products between the NiO_x HTL (as-deposited or UVO-treated) and organohalide salts we used high-resolution XPS. Details of the fitting procedures for the treated (UVO, FAI) and as-deposited NiO_x core levels (Ni 2p, I 3d, O 1s, N 1s and C 1s) are given in the SI (**Supplemental Note 1**). Representative Ni $2p_{3/2}$ core level spectra are shown in **Figures 3A and 3D** for as-deposited and UVO-treated NiO_x films, revealing treatment-dependent changes in the near-surface composition of the NiO_x surface. Chemical composition in the near surface region was estimated using previously published XPS results for a variety of NiO_x samples, in which fitting of the Ni 2p spectral envelope shows at least three distinct species.[19,59,60] The first three peaks in the binding energy (BE) region starting at ca. 852 eV are well-established contributions from NiO (red), $Ni(OH)_2$ (green), and NiOOH (blue). A fourth, high binding energy peak was required in the constrained fitting procedure and

here is classified as $Ni^{\geq 3+}$ (cyan), which could include Ni_2O_3, γ-NiOOH, or β-NiOOH, which has also been reported to have alternating Ni^{3+} and Ni^{4+} cations.[61] The relative Ni $2p_{3/2}$ composition for the samples in **Figure 3** is reported in **Table S1**, which neglects the high binding energy satellite peaks with binding energies above 860 eV that are associated with unscreened Ni components and are typically not used to fit Ni oxidation states.[19] In agreement with previous studies,[53] UVO treatment primarily led to a decrease in divalent NiO species and an increase in both the relative O/Ni ratio (**Table 2**) and the concentration of the highly reactive $Ni^{\geq 3+}$ defects.

Deposition of FAI onto the as-deposited and UVO NiO_x films resulted in a significant decrease (ca. 15-25 rel.%) in the $Ni^{\geq 3+}$ content, corroborating our hypothesis that under-coordinated nickel cations acted as oxidants (Lewis acid sites). These Ni $2p_{3/2}$-derived changes in the NiO_x film composition after various treatments were generally in agreement with those determined from analysis of the corresponding O 1s spectra (**Fig. S8, Table S2**). In addition, both the Ni $2p_{3/2}$ and O 1s spectra for the UVO-treated samples showed a significant increase (~0.3 eV) in binding energy after FAI treatment (**Tables S1 & S2**), indicating a shift in E_F away from the valence band maximum due to a decrease in concentration of $Ni^{\geq 3+}$ dopants. These changes in the NiO_x composition after FAI deposition were accompanied by the appearance of a I $3d_{5/2}$ signal in **Figures 3B and 3E**. Compared to as-deposited samples, a ~3x lower iodide content was found on the UVO-treated NiO_x samples that are $Ni^{\geq 3+}$-rich (**Table 2**). This indicated that the electrochemical reduction of $Ni^{\geq 3+}$ defects was facilitated by oxidation of iodide, where electron transfer led to the formation of I_3^-, which was in equilibrium with volatile $I_{2(g)}$ and could leave the surface, supporting the lower iodide content observed at the UVO-treated surface.

Importantly, a significant increase in the N 1s signal in **Figures 3C and 3F** after FAI deposition indicated the presence of deprotonated formamidine (CH_4N_2, FA), the conjugate base of the protonated formamidinium ($CH_5N_2^+$, FA^+) species, demonstrating that $Ni^{\geq 3+}$ defect sites may also show Brønsted acid/base character and deprotonate the amine cations.

Collectively, the experiments above suggest that the reaction between the perovskite and NiO_x will proceed as shown in the reactions below, where HA^+ is a protonated A-site cation ($CH_3NH_3^+$ or MA+, $CH_5N_2^+$ or FA^+) and A is the deprotonated A-site cation (CH_3NH_2, CH_4N_2).

Equation 1: $HAPbI_3 \leftrightarrow PbI_2 + HA^+ + I^-$

Equation 2: $HA^+ \leftrightarrow A_{(g)} + H^+$

Equation 3: $I^- \overset{I_3^-}{\leftrightarrow} \frac{1}{2}I_{2\,(g)} + e^-$

Equation 4: $Ni^{\geq 3+}O_x + e^- + H^+ \leftrightarrow Ni^{\geq 2+}O_xH$

Equation 5: $HAPbI_3 + Ni^{\geq 3+}O_x \leftrightarrow Ni^{\geq 2+}O_xH + PbI_2 + A_{(g)} + \frac{1}{2}I_{2\,(g)}$

The resulting A-site deficient or $PbI_{2-x}Br_x$-rich perovskite products are presumed to limit hole harvesting efficiencies in solar cells. However, we note that if either the oxidation or reduction half reaction is cut off by a change in solvent or precursor, then the overall reaction will not proceed. *These XPS measurements directly confirmed the hypothesis that $Ni^{\geq 3+}$ defects degrade the organohalide salt via an ET-PT mechanism.*

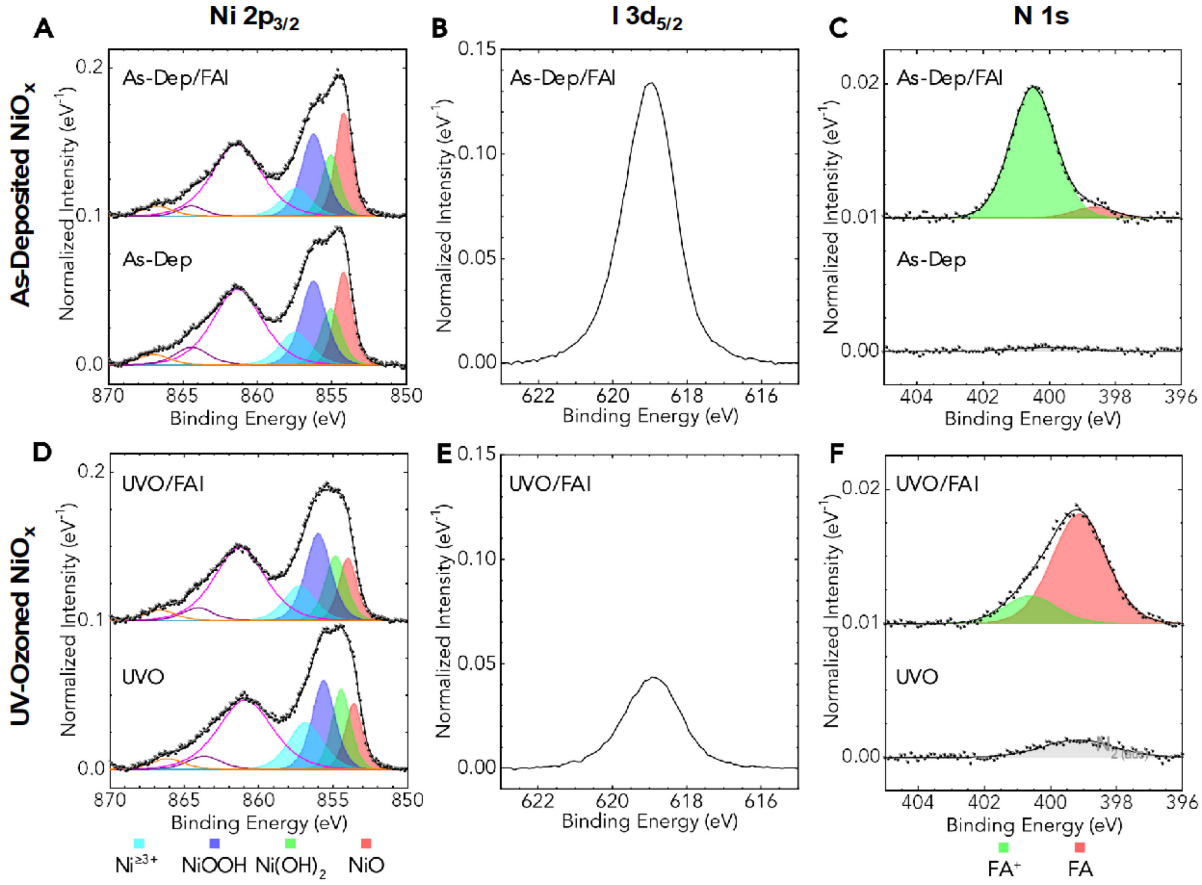

Figure 3 XPS Confirms Reaction Between Organohalides and NiO_x: X-ray photoelectron spectroscopy of as-deposited (A-C) and UV-ozone treated (D-F) NiO_x films. Nickel core level spectra of as-deposited (A) and UVO-treated (D) NiO_x films before (bottom) and after (top) being treated with FAI dissolved in DMF. Iodine core level

spectra of as-deposited (B) and UVO-treated (E) NiO_x films after treatment with FAI dissolved in DMF. Nitrogen core level spectra of as-deposited (C) and UVO-treated (F) NiO_x films before (bottom) and after (top) treatment with FAI dissolved in DMF.

Table 2: Near-surface atomic ratios of oxygen, nitrogen, carbon, and iodine compared to nickel for sputtered NiO_x as-deposited (As-dep) and with UV-ozone (UVO) treatment, with and without an FAI treatment. Additional near-surface atomic ratios for NiO_x treated with thermal annealing in air at 300 °C can be found in **Table S3**. Fitting for carbon species can be found in **Figure S10**.

Near-Surface Atomic Ratios

Sample	O/Ni	N/Ni	C/Ni	I/Ni
As-dep	1.08 ± 0.03	0.009 ± 0.001	0.70 ± 0.10	N/A
As-dep/FAI	1.06 ± 0.02	0.180 ± 0.010	0.80 ± 0.20	0.17 ± 0.01
UVO	1.33 ± 0.01	0.032 ± 0.005	1.33 ± 0.01	N/A
UVO/FAI	1.17 ± 0.01	0.211 ± 0.003	1.17 ± 0.01	0.06 ± 0.01

We extended these series of XRD and XPS measurements to other NiO_x preparation methods (nanoparticles) and treatments (annealing in air) to determine whether there is a processing method that would prevent the formation of the reactive $Ni^{\geq 3+}$ species. We saw a slight decrease in the $Ni^{\geq 3+}$ content in nanoparticles (3 rel.%) or upon annealing in air (6 rel.%) compared to sputtered as-deposited samples (**Fig. S11**, **Table S1**). Regardless of preparation method or treatment there was still a non-negligible amount of $Ni^{\geq 3+}$, which caused the formation of similar amounts of $PbI_{2-x}Br_x$ in perovskite films deposited on each type of NiO_x (**Fig. S12**). The fact that all NiO_x films studied here had some remaining $Ni^{\geq 3+}$ content in the film is consistent with the notion that intrinsic defects are necessary for charge transport.[36,62] *Therefore, we expect the reaction outlined above to happen in all NiO_x charge transport layers*. We also believe that this may be generalizable to any semi-transparent metal oxide contacts whose surfaces can act as both Brønsted acid/base and Lewis acid/base reactants toward perovskite precursors, an observation that has been made recently for TiO_2 and SnO_2 interlayers and contacts.[44–46]

Excess A-site Cation Improves V_{OC} of Perovskite Solar Cells on NiO_x

Having determined the cause of the reaction at the interface with the perovskite precursor, we then set out to identify ways to prevent the reaction from happening and improve device

performance in perovskite solar cells with NiO_x HTLs. In addition to processing changes and post-treatments, we hypothesized that a simpler approach is to alter the perovskite precursor stoichiometry to include excess A-site cation. This excess should offset the amount that is lost due to reaction with the NiO_x surface and therefore remove barriers to hole extraction and enhance V_{OC} and device performance (**Fig. 4A**). To test this, we fabricated a series of p-i-n perovskite solar cells with the device architecture glass/indium tin oxide (ITO)/NiO_x/$Cs_{0.25}FA_{0.75}Pb(Br_{0.2}I_{0.8})_3$ perovskite/LiF/C_{60}/bathocuproine (BCP)/Ag using different molar amounts of excess A-site in the perovskite. With excess A-site cation incorporated, perovskites deposited on NiO_x show no residual $PbI_{2-x}Br_x$ and a recovery of lattice parameters to equal that of FACs on organic HTLs (**Fig. 4B**). Adding 1-3 mol.% of excess A-site cation resulted in drastic improvements in open circuit voltage from 0.92 V up to 1.15 V and overall device performance from 15.06% to 19.66% PCE (**Fig. 4C & D, Table 3**). We found a consistent increase in V_{OC} up to about 3 mol.% excess FA^+, after which devices suffered from a decrease in fill factor (FF) and current (J_{SC}) with continued increase in A-site cation (**Figures S13 & S14**). The champion device with 3 mol.% excess FAI had a V_{OC} of 1.14 V, J_{SC} of 20.34 mA/cm^2, and FF of 85.0%, resulting in a PCE of 19.66% with minimal hysteresis and a steady-state maximum power point of 19.67% (**Figure 4D, Table 3, EQE in Figure S15**). We found these results to be reproducible across months of experiments.

Importantly, adding FAI, FABr, CsI, and CsBr as excess A-site cations within the precursor all resulted in the same improvement in V_{OC} (**Figure S16**), despite the fact we did not find inorganic and bromide precursors to react with NiO_x (**Figure 2**). This result highlights that the goal of this strategy was to provide additional A-site cations to compensate the formation of $PbI_{2-x}Br_x$ at the perovskite/NiO_x interface, not to alter the energetics or chemical composition of the NiO_x. The importance of replacing the A-site cation over incorporating excess halide was confirmed by the fact that the use of excess PbI_2 had no effect on the V_{OC} (**Figure S14**). Scanning electron microscopy images showed almost no change between the perovskite with and without excess organic cation, removing the possibility of any effect of increase in apparent grain domain size on the performance improvement (**Figure S3**).

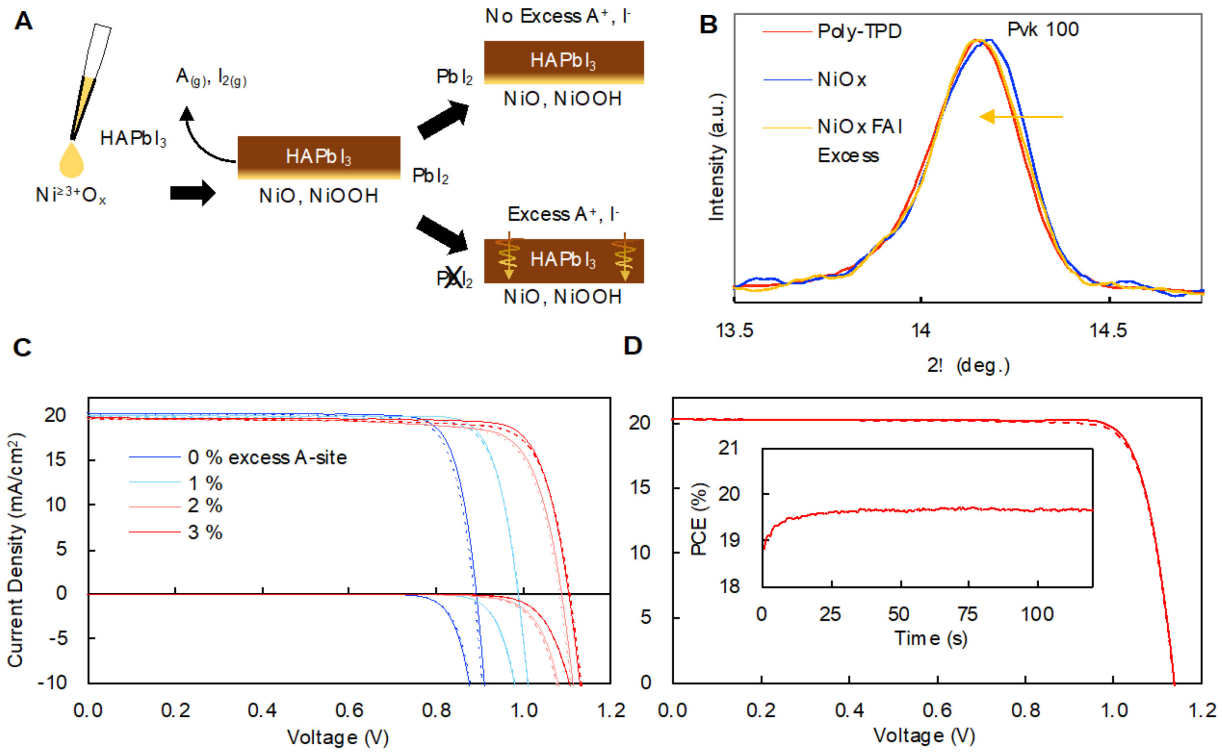

Figure 4 Excess A-site Cation Improves V_{OC} of Perovskite Solar Cells on NiO_x: (A) Schematic of the addition of excess A-site to the perovskite precursor which titrates reactive sites at the NiO_x surface, preventing the formation of $PbI_{2-x}Br_x$ at the interface. (B) XRD of perovskite films on NiO_x with excess A-site in mol.% in the precursor solution showing a shift in the (100) perovskite peak. (C) Dark and light J-V curves of $Cs_{0.25}FA_{0.75}Pb(Br_{0.2}I_{0.8})_3$ perovskite solar cells with 0-3 mol.% excess A-site. (D) J-V curves of the champion $Cs_{0.25}FA_{0.75}Pb(Br_{0.2}I_{0.8})_3$ wide band gap perovskite solar cell with 3 mol.% excess A-site cation with 19.7% power conversion efficiency. Inset is the maximum power point tracking data, showing a stabilized power output of 19.7%. Solid lines correspond to the reverse scan and dashed lines are the forward scan.

Table 3: Current-voltage parameters including open-circuit voltage (V_{OC}), short-circuit current (J_{SC}), fill factor (FF), and power conversion efficiency (η) of champion solar cells with and without excess A-site cation in the perovskite precursor. For the champion device (champ) the values for both the forward (Fwd) and reverse (Rvs) scans are shown, as well as the stabilized maximum power point (MPP) output.

Solar Cell	V_{OC} (V)	J_{SC} (mA/cm^2)	FF (%)	η (%)
Control	0.92	20.40	79.9	15.06
3% A-Site Best V_{OC}	1.15	19.56	84.7	19.06
3% A-Site Champ (Fwd)	1.14	20.35	83.9	19.40
3% A-Site Champ (Rvs)	1.14	20.34	85.0	19.66

3% A-Site Champ (MPP)	19.67

We extended this method to the high-performance $Cs_{0.05}MA_{0.16}FA_{0.79}Pb_{1.03}(Br_{0.16}I_{0.86})_3$ (triple cation) composition, and found that upon the addition of excess A-site the PCE was improved from 15.2% to 18.2% due to a V_{OC} improvement from 0.95 V to 1.05 V, similar to our control triple cation devices on PTAA HTLs (**Fig. S17 and Table S4**). Because triple cation perovskites are typically fabricated with about 3 mol.% excess PbI_2,[49] and due to the increased propensity for methylammonium to be deprotonated over formamidinium, up to 8 mol.% excess A-site was needed for optimum performance (5 mol.% excess if you consider the 3 mol.% excess PbI_2 in the initial recipe). We also successfully extended this method to different types of NiO_x and found similar V_{OC} improvements on NiO_x layers deposited using sol-gel precursors, ALD, and nanoparticle dispersions (**Fig. S18**). As expected, the amount of excess A-site necessary to counteract the formation of $PbI_{2-x}Br_x$ at the NiO_x interface must be tuned for different NiO_x processing routes based on the amount of intrinsic $Ni^{\geq 3+}$ defects present. We note that pre-treating the NiO_x surface with FAI to remove the harmful defects before perovskite deposition, also resulted in improved V_{OC} (**Fig. S19**). A recent study has also tried a similar route with vapor annealing of the perovskite film on NiO_x with organo-halide vapor, expanding the potential processing routes to prevent this problem.[63]

We emphasize that the reaction with $Ni^{\geq 3+}$ species occurs regardless of any excess A-site cation, meaning that the NiO_x surface quality is unchanged. Therefore, unlike previous reports, which attribute V_{OC} improvements to changes in the band alignment and/or surface passivation of NiO_x, we show that the main cause for PCE loss is the formation of $PbI_{2-x}Br_x$-rich perovskite at the interface. Prior efforts likely unknowingly mitigated this problem by passivation of $Ni^{\geq 3+}$ defects prior to perovskite deposition.

Drift-Diffusion Modeling Identifies Removal of a Hole Extraction Barrier and Reduction in Surface Recombination

To further understand the changes in V_{OC}, we set about linking the chemistry of the reactions above to device physics, specifically to explain how $PbI_{2-x}Br_x$ might limit V_{OC} and how addition of excess A-site cation to the perovskite precursor improves device V_{OC} and PCE. Here, we determined the electronic defectivity of perovskite solar cells through external radiative

efficiency (ERE) measurements, which show the quasi-Fermi level splitting (QFLS) of an absorber material (see Methods for description of ERE measurements).[64,65] This value will depend on both the quality of the absorber itself and the surface recombination at the absorber/contact interfaces, where a higher surface recombination will lead to lower ERE. From the QFLS of the absorber, one can derive the implied voltage (iV_{OC}) of the device, which is the maximum V_{OC} that can be obtained assuming no barriers to charge extraction (*i.e.*, perfectly selective contacts). Interestingly, we found that the iV_{OC} (**Table 4**) of perovskite devices was weakly dependent on the HTM (PTAA, poly-TPD, or NiO_x), suggesting that poor perovskite passivation by the HTM is not the reason for the V_{OC} losses on NiO_x. Upon adding excess A-site cation to the perovskite ink, the iV_{OC} improved slightly, suggesting a potential reduction in surface recombination, but not enough to fully explain the differences in V_{OC}.

Table 4: Average values and standard deviations of open-circuit voltage (V_{OC}), external radiative efficiency (ERE), and implied open-circuit voltage (iV_{OC}) of $Cs_{0.25}FA_{0.75}Pb(Br_{0.2}I_{0.8})_3$ perovskite solar cells on various hole transport layers (HTLs).

HTL	V_{OC} (V)	ERE (%)	iV_{OC} (V)
Poly-TPD	1.11 ± 0.02	0.038 ± 0.019	1.20 ± 0.02
PTAA	1.12 ± 0.02	0.023 ± 0.015	1.18 ± 0.02
NiO_x	0.94 ± 0.02	0.018 ± 0.004	1.18 ± 0.00
NiO_x Excess A-site	1.13 ± 0.02	0.054 ± 0.024	1.20 ± 0.01

We then turned to understanding how the $PbI_{2-x}Br_x$ rich perovskite influences charge extraction at the perovskite/NiO_x interface by using a recently published open-source drift-diffusion model that incorporates ionic mobilities into the electrical properties of the perovskite solar cell.[66]. We hypothesized that the defective perovskite acts as a hole extraction barrier, preventing equilibration of the quasi-Fermi level of holes in the NiO_x and the perovskite. This barrier to hole extraction may be due to an energetic barrier of the defective perovskite or lower hole mobility through the defective perovskite region at the NiO_x interface. Briefly, we modeled the impact of an extraction barrier to holes at open circuit conditions by altering the hole extraction velocity at the HTL/perovskite interface as a proxy, while keeping all else constant and assuming a perfect electron contact at the ETL/perovskite interface. The parameters used in

the model are listed in **Table S5**. The model demonstrates that with a $PbI_{2-x}Br_x$ extraction barrier, the hole quasi-Fermi level in NiO_x does not equilibrate with that in the perovskite, as shown in **Figure 5A**, leading to a situation in which the device V_{OC} (**Figure 5B**) is much less than the iV_{OC}, correlating with experimental results. Removal of that extraction barrier, as we have done experimentally though the addition of excess A-site, improves the V_{OC} (**Figure 5D**), nearly approaching the iV_{OC} (**Table 4**) by reaching a hole quasi-Fermi level equilibrium between NiO_x and the perovskite (**Figure 5C**). The extraction barrier due to a $PbI_{2-x}Br_x$ "blocking layer" as we have modeled here will lead to an increase in hole density at the $PbI_{2-x}Br_x$/perovskite interface (and a decrease in the hole density at the $PbI_{2-x}Br_x/NiO_x$ interface) causing an increase in surface recombination at the $PbI_{2-x}Br_x$/perovskite interface. Without additional surface recombination, an s-kink as shown in the gray curve in **Figure 5B** would arise from a delay in carrier extraction and recombination due to the extraction barrier, which would actually improve the iV_{OC} in the absorber. However, we do not see an s-kink in JV curves, and we see a reproducible slight increase in iV_{OC} upon removal of the extraction barrier with excess A-site cation. Therefore, in our devices carriers that build up at the $PbI_{2-x}Br_x$/perovskite interface due to the extraction barrier recombine, and the s-kink is hidden by larger surface recombination at the $PbI_{2-x}Br_x$/perovskite interface. In summary, with both an extraction barrier and increased surface recombination, we can successfully reproduce both the large difference between iV_{OC} and V_{OC} observed experimentally (**Table 4**) and the significant V_{OC} drop without much change in FF and J_{SC} experimentally seen (compare blue curves in **Figures 4B & 5B**).

Previous studies have reported that excess PbI_2 helps to reduce defect concentration and promote crystal formation in perovskite films leading to higher device efficiencies,[51,52] which appears to be in direct contradiction with our claims in this study: that A-site deficient, $PbI_{2-x}Br_x$-rich perovskite reduces voltage in devices with NiO_x HTLs. We speculate that this may be due to several reasons, all of which should be investigated further. (1) The defective perovskite in this study is A-site deficient and $PbI_{2-x}Br_x$-rich, but it is not necessarily pure $PbI_{2-x}Br_x$. It could be that a defective perovskite region with A-site defects is more detrimental to device performance than small amounts of pure PbI_2. (2) PbI_2 excess added to solution likely resides in local regions at grain boundaries, whereas in this study the $PbI_{2-x}Br_x$ almost certainly forms via an ET-PT reaction at the NiO_x interface, where it acts as a barrier to charge extraction.

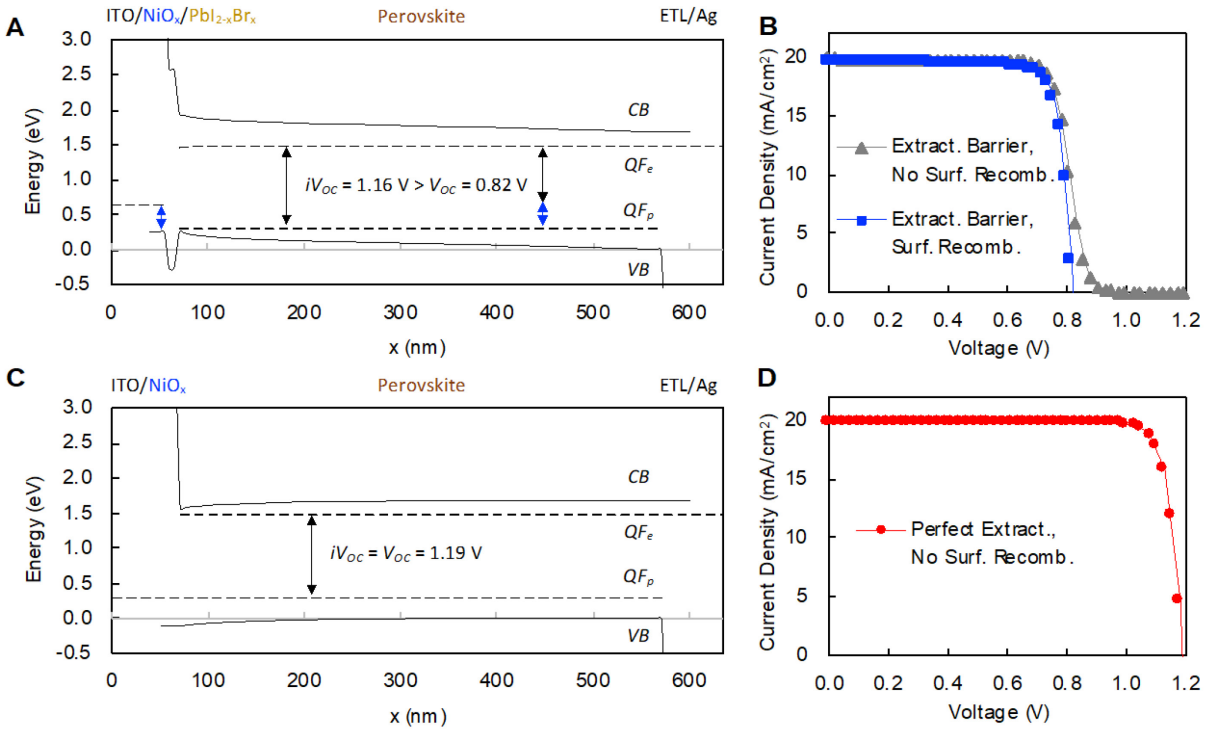

Figure 5 Modeling Extraction Barriers at the NiO_x/Perovskite Interface: (A) Simulated band diagram of a p-i-n perovskite solar cell at open circuit, accounting for mobile ions, with a perfect electron transport layer (ETL) contact (no surface recombination and perfect electron extraction) with a $PbI_{2-x}Br_x$ extraction barrier at the NiO_x/perovskite interface and the (B) simulated JV curves with (blue) and without (gray) surface recombination. Blue arrows show the V_{OC} loss due to an extraction barrier at the NiO_x interface. (C) Simulated band diagram of the p-i-n perovskite solar cell at open circuit with a perfect ETL and NiO_x interface and the (D) simulated JV curve.

Long-Term Stablity of Perovskite Solar Cells with NiO_x and Organic HTLs

Finally, we performed long-term operational stability tests to determine if the reaction would continue to occur or be self-limited by the consumption of $Ni^{\geq 3+}$ species at the surface during initial perovskite film formation. We first tested the devices for thermal stability to accelerate potential reaction kinetics at the interface. We made p-i-n solar cells with and without excess organic cation on NiO_x or poly-TPD. Unencapsulated devices with gold contacts were placed on a hotplate at 85 °C in a nitrogen glovebox for 2000 hours, a test that we have found approximates the standard damp heat test assuming excellent packaging.[29,30,33] As expected given previous reports of good stability with NiO_x HTLs,[30,67] cells on NiO_x with or without excess A-site cation actually improved in initial V_{OC} after aging. Furthermore, cells on NiO_x HTLs outperformed their organic counterparts, maintaining on average 91% and 97% of their initial

efficiency with or without excess A-site, respectively, compared to cells on organic poly-TPD layers, which only maintained an average of 67% of their initial efficiency (**Figure 6A,B and Table S6**). These stability results imply that the deprotonation reaction of the organic cation by $Ni^{\geq 3+}$ species is a self-limiting reaction that only occurs during initial film formation, making the use of excess A-site cation a route towards both highly efficient and stable solar cells on NiO_x HTLs. We also performed long-term operational stability testing on unencapsulated devices in nitrogen at 0.77 sun illumination and 55 °C (**Figure 6C**). Devices with NiO_x with or without excess A-site cation maintained >80% if their initial efficiency after 400 hours, as compared to a device with a poly-TPD hole transport layer, which degraded to less than 50% of its initial efficiency over the same time period. We speculate that additional studies could show the removal of excess $PbI_{2-x}Br_x$ to be beneficial for long-term operational stability, given recent reports indicating that excess PbI_2 can photocatalyze degradation in perovskite solar cells.[68]

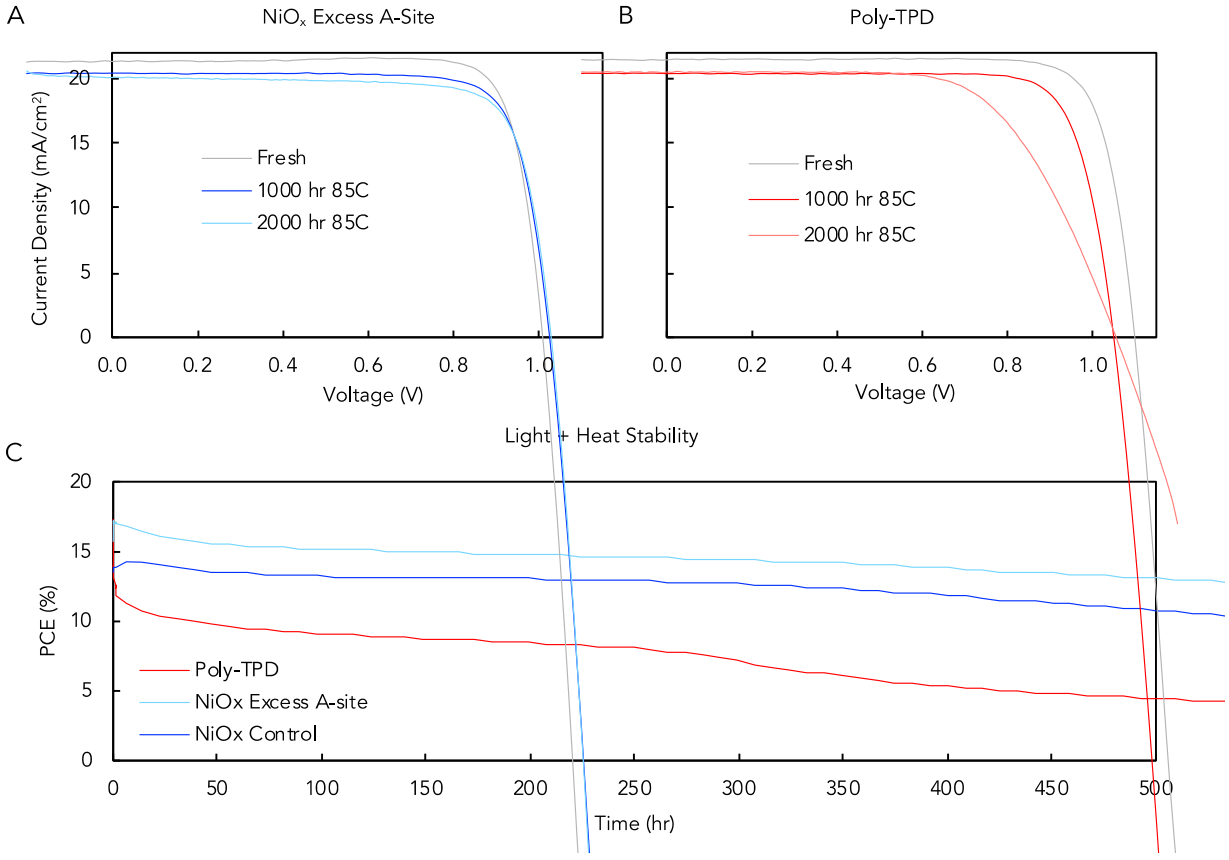

Figure 6 Long-Term Stablity of Perovskite Solar Cells with NiO_x and Organic HTLs: (A), (B) JV curves before and after thermal stability testing of a $Cs_{0.25}FA_{0.75}Pb(Br_{0.2}I_{0.8})_3$ perovskite with (A) excess A-site on NiO_x and (B) a control solution on poly-TPD for 2000 hours at 85 °C. (C) Maximum power point tracking to compare stability of

unencapsulated perovskite solar cells using NiO_x hole transport layers with and without excess A-site cation with poly-TPD at 0.77 suns and 55 °C in a sealed chamber under N_2.

Conclusion

In summary, we have shown that NiO_x $Ni^{\geq 3+}$ surface species react with perovskite organo-iodide precursors via an electron transfer-proton transfer mechanism. This reaction results in the formation of defective, $PbI_{2-x}Br_x$-rich, A-site cation-deficient perovskite at the NiO_x interface. This defective perovskite forms an energetic barrier to hole extraction and increases recombination at the interface, resulting in V_{OC} losses in devices.

This reaction mechanism and V_{OC} loss is general to many NiO_x types, regardless of processing conditions, and several common perovskite active layers. We present two strategies to prevent this reaction from occurring when fabricating perovskite solar cells: (1) A-site post-treatments to the NiO_x HTL or (2) use of excess A-site in the perovskite precursor solution to counteract the loss in organohalide that occurs during this reaction. Whereas post-treatments to the NiO_x remove reactive $Ni^{\geq 3+}$ sites before perovskite deposition, the use of excess A-site cation acts to compensate for organic cation that is lost due to reaction with the NiO_x, reforming high quality perovskite active layer at the interface. Many previous reports have used surface treatments with various chemicals, without realizing the mechanism at play. Unlike surface treatments, which are sensitive to the $Ni^{\geq 3+}$ defect density and therefore the processing parameters of the NiO_x, we show the addition of excess A-site to be a universal strategy that is generalizable to multiple types of NiO_x and multiple perovskite active layers. Furthermore, we posit that this may be a more general finding for all semi-transparent metal oxide contacts, such as TiO_2 or SnO_2, where their surfaces can act as both Brønsted acid/base and Lewis acid/base reactants toward perovskite precursors. Indeed, a recent study has shown that spincasting the perovskite precursor on TiO_2 or SnO_2 contacts multiple times improves efficiency of devices – an initial precursor deposition could consume reactive sites at the oxide surface and a secondary deposition would then form less-defective perovskite.[69]

Experimental Procedures

Experimental Procedures can be found in the Supplemental Information.

Acknowledgments
We would like to thank Professor Yong-Hang Zhang and his team, in particular Tyler McCarthy and Jia Ding, for building and providing access to the ERE measurement tool.

Funding: This material is based upon work supported by the U.S. Department of Energy's Office of Energy Efficiency and Renewable Energy (EERE) under Solar Energy Technologies Office (SETO) Agreement Numbers DE-EE0008167 and DE-EE0008552. This project was partially supported by the Office of Naval Research under award numbers N00014-17-1-2525 and N00014-18-1-2711. Salary support for R.C.S. came both from ONR N00014-18-1-2711 and from the Office for Research, Innovation and Impact (RII) at the University of Arizona. C.C.B. acknowledges support from the National Science Foundation Graduate Research Fellowship under Grant No. DGE-1656518. Z.H. and S.K. acknowledge support by the National Science Foundation Award Number 1846685. T.M. and J.M.L acknowledge the Operational Energy Capability Improvement Fund of the Department of Defense. C.C. acknowledges support from the U.S. Department of Energy Science Undergraduate Laboratory Internship Program. This work was authored in part by the National Renewable Energy Laboratory, operated by Alliance for Sustainable Energy, LLC, for the U.S. Department of Energy (DOE) under Contract No. DE-AC36-08GO28308. The views expressed in the article do not necessarily represent the views of the DOE or the U.S. Government. The U.S. Government retains and the publisher, by accepting the article for publication, acknowledges that the U.S. Government retains a nonexclusive, paid-up, irrevocable, worldwide license to publish or reproduce the published form of this work, or allow others to do so, for U.S. Government purposes.

Author contributions: Conceptualization, C.C.B., R.C.S., N.R.A., M.D.M.; Formal analysis, C.C.B., R.C.S, L.B., A.O., S.K., E.J.W., E.L.R.; Funding acquisition, J.J.B., S.F.B., Z.C.H., J.M.L., E.L.R., N.R.A., M.D.M.; Investigation, C.C.B., R.C.S., T.M., R.K., L.B., A.O., S.K., C.C., E.J.W., J.W., J.A.R., C.P., A.F.P., Z.J.Y.; Methodology, C.C.B., R.C.S., T.M., R.K., L.B., A.O., S.K., C.C., E.J.W., J.A.R., C.P., A.F.P., Z.J.Y.; Project administration, N.R.A., M.D.M.; Software, L.B., J.W.; Supervision, N.R.A., M.D.M.; Validation, T.M., R.K.; Visualization, C.C.B., Writing – original draft, C.C.B. Writing – review & editing, all authors.
Declaration of Interests: M.D.M is an advisor to Swift Solar. A.F.P. and M.D.M. are inventors on patent application PCT/US2017/051753 submitted by Stanford University that covers the atomic layer deposition of contacts used in this work.

References

1. Green, M.A., Dunlop, E.D., Hohl-Ebinger, J., Yoshita, M., Kopidakis, N., and Ho-Baillie, A.W.Y. (2020). Solar cell efficiency tables (Version 55). Prog. Photovoltaics Res. Appl. *28*, 3–15.
2. Green, M.A., Ho-Baillie, A., and Snaith, H.J. (2014). The emergence of perovskite solar cells. Nat. Photonics *8*, 506–514.
3. Berry, J.J., van de Lagemaat, J., Al-Jassim, M.M., Kurtz, S., Yan, Y., and Zhu, K. (2017). Perovskite Photovoltaics: The Path to a Printable Terawatt-Scale Technology. ACS Energy Lett. *2*, 2540–2544.
4. Irwin, M.D., Buchholz, D.B., Hains, A.W., Chang, R.P.H., and Marks, T.J. (2008). p-Type semiconducting nickel oxide as an efficiency-enhancing anode interfacial layer in polymer bulk-heterojunction solar cells. Proc. Natl. Acad. Sci. *105*, 2783–2787.
5. Steirer, K.X., Ndione, P.F., Widjonarko, N.E., Lloyd, M.T., Meyer, J., Ratcliff, E.L., Kahn, A., Armstrong, N.R., Curtis, C.J., Ginley, D.S., et al. (2011). Enhanced efficiency in plastic solar cells via energy matched solution processed NiOxinterlayers. Adv. Energy Mater. *1*, 813–820.

6. Steirer, K.X., Chesin, J.P., Widjonarko, N.E., Berry, J.J., Miedaner, A., Ginley, D.S., and Olson, D.C. (2010). Solution deposited NiO thin-films as hole transport layers in organic photovoltaics. Org. Electron. *11*, 1414–1418.
7. Berry, J.J., Widjonarko, N.E., Bailey, B.A., Sigdel, A.K., Ginley, D.S., and Olson, D.C. (2010). Surface Treatment of NiO Hole Transport Layers for Organic Solar Cells. IEEE J. Sel. Top. Quantum Electron. *16*, 1649–1655.
8. Widjonarko, N.E., Ratcliff, E.L., Perkins, C.L., Sigdel, A.K., Zakutayev, A., Ndione, P.F., Gillaspie, D.T., Ginley, D.S., Olson, D.C., and Berry, J.J. (2012). Sputtered nickel oxide thin film for efficient hole transport layer in polymer–fullerene bulk-heterojunction organic solar cell. Thin Solid Films *520*, 3813–3818.
9. Chen, W., Zhou, Y., Chen, G., Wu, Y., Tu, B., Liu, F.Z., Huang, L., Ng, A.M.C., Djurišić, A.B., and He, Z. (2019). Alkali Chlorides for the Suppression of the Interfacial Recombination in Inverted Planar Perovskite Solar Cells. Adv. Energy Mater. *9*, 1803872.
10. You, J., Meng, L., Song, T. Bin, Guo, T.F., Chang, W.H., Hong, Z., Chen, H., Zhou, H., Chen, Q., Liu, Y., et al. (2016). Improved air stability of perovskite solar cells via solution-processed metal oxide transport layers. Nat. Nanotechnol. *11*, 75–81.
11. Chen, W., Liu, F.Z., Feng, X.Y., Djurišić, A.B., Chan, W.K., and He, Z.B. (2017). Cesium Doped NiOx as an Efficient Hole Extraction Layer for Inverted Planar Perovskite Solar Cells. Adv. Energy Mater. *7*, 1700722.
12. Bi, E., Chen, H., Xie, F., Wu, Y., Chen, W., Su, Y., Islam, A., Grätzel, M., Yang, X., and Han, L. (2017). Diffusion engineering of ions and charge carriers for stable efficient perovskite solar cells. Nat. Commun. *8*, 15330.
13. Chen, W., Wu, Y., Yue, Y., Liu, J., Zhang, W., Yang, X., Chen, H., Bi, E., Ashraful, I., Grätzel, M., et al. (2015). Efficient and stable large-area perovskite solar cells with inorganic charge extraction layers. Science *350*, 944–948.
14. Wang, Q., Chueh, C., Zhao, T., Cheng, J., Eslamian, M., Choy, W.C.H., and Jen, A.K. -Y. (2017). Effects of Self-Assembled Monolayer Modification of Nickel Oxide Nanoparticles Layer on the Performance and Application of Inverted Perovskite Solar Cells. ChemSusChem *10*, 3794–3803.
15. Yao, K., Li, F., He, Q., Wang, X., Jiang, Y., Huang, H., and Jen, A.K.Y. (2017). A copper-doped nickel oxide bilayer for enhancing efficiency and stability of hysteresis-free inverted mesoporous perovskite solar cells. Nano Energy *40*, 155–162.
16. He, Q., Yao, K., Wang, X., Xia, X., Leng, S., and Li, F. (2017). Room-Temperature and Solution-Processable Cu-Doped Nickel Oxide Nanoparticles for Efficient Hole-Transport Layers of Flexible Large-Area Perovskite Solar Cells. ACS Appl. Mater. Interfaces *9*, 41887–41897.
17. Di Girolamo, D., Phung, N., Jošt, M., Al-Ashouri, A., Chistiakova, G., Li, J., Márquez, J.A., Unold, T., Korte, L., Albrecht, S., et al. (2019). From Bulk to Surface: Sodium Treatment Reduces Recombination at the Nickel Oxide/Perovskite Interface. Adv. Mater. Interfaces *6*, 1900789.
18. Di Girolamo, D., Matteocci, F., Kosasih, F.U., Chistiakova, G., Zuo, W., Divitini, G., Korte, L., Ducati, C., Di Carlo, A., Dini, D., et al. (2019). Stability and Dark Hysteresis Correlate in NiO-Based Perovskite Solar Cells. Adv. Energy Mater. *9*, 1901642.
19. Ratcliff, E.L., Meyer, J., Steirer, K.X., Garcia, A., Berry, J.J., Ginley, D.S., Olson, D.C., Kahn, A., and Armstrong, N.R. (2011). Evidence for near-surface NiOOH species in solution-processed NiOx selective interlayer materials: Impact on energetics and the

performance of polymer bulk heterojunction photovoltaics. Chem. Mater. *23*, 4988–5000.
20. Steirer, K.X., Richards, R.E., Sigdel, A.K., Garcia, A., Ndione, P.F., Hammond, S., Baker, D., Ratcliff, E.L., Curtis, C., Furtak, T., et al. (2015). Nickel oxide interlayer films from nickel formate-ethylenediamine precursor: Influence of annealing on thin film properties and photovoltaic device performance. J. Mater. Chem. A *3*, 10949–10958.
21. Scheideler, W.J., Rolston, N., Zhao, O., Zhang, J., and Dauskardt, R.H. (2019). Rapid Aqueous Spray Fabrication of Robust NiO_x : A Simple and Scalable Platform for Efficient Perovskite Solar Cells. Adv. Energy Mater. *9*, 1803600.
22. Jošt, M., Bertram, T., Koushik, D., Marquez, J.A., Verheijen, M.A., Heinemann, M.D., Köhnen, E., Al-Ashouri, A., Braunger, S., Lang, F., et al. (2019). 21.6%-Efficient Monolithic Perovskite/Cu(In,Ga)Se_2 Tandem Solar Cells with Thin Conformal Hole Transport Layers for Integration on Rough Bottom Cell Surfaces. ACS Energy Lett. *4*, 583–590.
23. Seo, S., Jeong, S., Bae, C., Park, N.G., and Shin, H. (2018). Perovskite Solar Cells with Inorganic Electron- and Hole-Transport Layers Exhibiting Long-Term (≈500 h) Stability at 85 °C under Continuous 1 Sun Illumination in Ambient Air. Adv. Mater. *30*, 1801010.
24. Aydin, E., Troughton, J., De Bastiani, M., Ugur, E., Sajjad, M., Alzahrani, A., Neophytou, M., Schwingenschlögl, U., Laquai, F., Baran, D., et al. (2018). Room-Temperature Sputtered Nanocrystalline Nickel Oxide as Hole Transport Layer for p−i−n Perovskite Solar Cells. ACS Appl. Energy Mater. *1*, 6227–6233.
25. Azens, A., Kullman, L., Vaivars, G., Nordborg, H., and Granqvist, C.G. (1998). Sputter-deposited nickel oxide for electrochromic applications. Solid State Ionics *113–115*, 449–456.
26. Li, G., Jiang, Y., Deng, S., Tam, A., Xu, P., Wong, M., and Kwok, H.S. (2017). Overcoming the Limitations of Sputtered Nickel Oxide for High-Efficiency and Large-Area Perovskite Solar Cells. Adv. Sci. *4*, 1700463.
27. Xu, J., Boyd, C.C., Yu, Z.J., Palmstrom, A.F., Witter, D.J., Larson, B.W., France, R.M., Werner, J., Harvey, S.P., Wolf, E.J., et al. (2020). Triple-halide wide-band gap perovskites with suppressed phase segregation for efficient tandems. Science *367*, 1097–1104.
28. Hou, Y., Aydin, E., Bastiani, M. De, Xiao, C., Isikgor, F.H., Xue, D.-J., Chen, B., Chen, H., Bahrami, B., Chowdhury, A.H., et al. (2020). Efficient tandem solar cells with solution-processed perovskite on textured crystalline silicon. Science *367*, 1135–1140.
29. Boyd, C.C., Cheacharoen, R., Leijtens, T., and McGehee, M.D. (2019). Understanding Degradation Mechanisms and Improving Stability of Perovskite Photovoltaics. Chem. Rev. *119*, 3418–3451.
30. Boyd, C.C., Cheacharoen, R., Bush, K.A., Prasanna, R., Leijtens, T., and McGehee, M.D. (2018). Barrier Design to Prevent Metal-Induced Degradation and Improve Thermal Stability in Perovskite Solar Cells. ACS Energy Lett. *3*, 1772–1778.
31. Cheacharoen, R., Boyd, C.C., Burkhard, G.F., Leijtens, T., Raiford, J.A., Bush, K.A., Bent, S.F., and McGehee, M.D. (2018). Encapsulating perovskite solar cells to withstand damp heat and thermal cycling. Sustain. Energy Fuels *2*, 2398–2406.
32. Bush, K.A., Bailie, C.D., Chen, Y., Bowring, A.R., Wang, W., Ma, W., Leijtens, T., Moghadam, F., and McGehee, M.D. (2016). Thermal and environmental stability of semi-transparent perovskite solar cells for tandems by a solution-processed nanoparticle buffer layer and sputtered ITO electrode. Adv. Mater. *28*, 3937–3943.
33. Cheacharoen, R., Rolston, N.J., Harwood, D., Bush, K.A., Dauskardt, R.H., and

McGehee, M.D. (2018). Design and understanding of encapsulated perovskite solar cells to withstand temperature cycling. Energy Environ. Sci. *11*, 144–150.
34. Cheng, Y., Li, M., Liu, X., Cheung, S.H., Chandran, H.T., Li, H.W., Xu, X., Xie, Y.M., So, S.K., Yip, H.L., et al. (2019). Impact of surface dipole in NiOx on the crystallization and photovoltaic performance of organometal halide perovskite solar cells. Nano Energy *61*, 496–504.
35. Bai, S., Da, P., Li, C., Wang, Z., Yuan, Z., Fu, F., Kawecki, M., Liu, X., Sakai, N., Wang, J.T.-W., et al. (2019). Planar perovskite solar cells with long-term stability using ionic liquid additives. Nature *571*, 245–250.
36. Traore, B., Pedesseau, L., Blancon, J.C., Tretiak, S., Mohite, A.D., Even, J., Katan, C., and Kepenekian, M. (2020). Importance of Vacancies and Doping in the Hole-Transporting Nickel Oxide Interface with Halide Perovskites. ACS Appl. Mater. Interfaces *12*, 6633–6640.
37. Belisle, R.A., Jain, P., Prasanna, R., Leijtens, T., and McGehee, M.D. (2016). Minimal Effect of the Hole-Transport Material Ionization Potential on the Open-Circuit Voltage of Perovskite Solar Cells. ACS Energy Lett. *1*, 556–560.
38. Dänekamp, B., Droseros, N., Tsokkou, D., Brehm, V., Boix, P.P., Sessolo, M., Banerji, N., and Bolink, H.J. (2019). Influence of hole transport material ionization energy on the performance of perovskite solar cells. J. Mater. Chem. C *7*, 523–527.
39. Heo, J.H., Im, S.H., Noh, J.H., Mandal, T.N., Lim, C.-S., Chang, J.A., Lee, Y.H., Kim, H., Sarkar, A., Nazeeruddin, M.K., et al. (2013). Efficient inorganic–organic hybrid heterojunction solar cells containing perovskite compound and polymeric hole conductors. Nat. Photonics *7*, 486–491.
40. Sun, Q., Wang, Y.A., Li, L.S., Wang, D., Zhu, T., Xu, J., Yang, C., and Li, Y. (2007). Bright, multicoloured light-emitting diodes based on quantum dots. Nat. Photonics *1*, 717–722.
41. Wang, J., Fu, W., Jariwala, S., Sinha, I., Jen, A.K.-Y., and Ginger, D.S. (2019). Reducing Surface Recombination Velocities at the Electrical Contacts Will Improve Perovskite Photovoltaics. ACS Energy Lett. *4*, 222–227.
42. Yang, J., Siempelkamp, B.D., Mosconi, E., De Angelis, F., and Kelly, T.L. (2015). Origin of the Thermal Instability in CH3NH3PbI3 Thin Films Deposited on ZnO. Chem. Mater. *27*, 4229–4236.
43. Cheng, Y., Yang, Q.-D., Xiao, J., Xue, Q., Li, H.-W., Guan, Z., Yip, H.-L., and Tsang, S.-W. (2015). Decomposition of Organometal Halide Perovskite Films on Zinc Oxide Nanoparticles. ACS Appl. Mater. Interfaces *7*, 19986–19993.
44. Shallcross, R.C., Olthof, S., Meerholz, K., and Armstrong, N.R. (2019). Impact of Titanium Dioxide Surface Defects on the Interfacial Composition and Energetics of Evaporated Perovskite Active Layers. ACS Appl. Mater. Interfaces *11*, 32500–32508.
45. Kerner, R.A., and Rand, B.P. (2017). Linking Chemistry at the TiO_2/$CH_3NH_3PbI_3$ Interface to Current–Voltage Hysteresis. J. Phys. Chem. Lett. *8*, 2298–2303.
46. Hu, T., Becker, T., Pourdavoud, N., Zhao, J., Brinkmann, K.O., Heiderhoff, R., Gahlmann, T., Huang, Z., Olthof, S., Meerholz, K., et al. (2017). Indium-Free Perovskite Solar Cells Enabled by Impermeable Tin-Oxide Electron Extraction Layers. Adv. Mater. *29*, 1606656.
47. Bush, K.A., Frohna, K., Prasanna, R., Beal, R.E., Leijtens, T., Swifter, S.A., and Mcgehee, M.D. (2018). Compositional Engineering for Efficient Wide Band Gap

Perovskites with Improved Stability to Photoinduced Phase Segregation. ACS Energy Lett *3*, 8.
48. Bush, K.A., Manzoor, S., Frohna, K., Yu, Z.J., Raiford, J.A., Palmstrom, A.F., Wang, H.P., Prasanna, R., Bent, S.F., Holman, Z.C., et al. (2018). Minimizing Current and Voltage Losses to Reach 25% Efficient Monolithic Two-Terminal Perovskite-Silicon Tandem Solar Cells. ACS Energy Lett. *3*, 2173–2180.
49. Saliba, M., Matsui, T., Seo, J.-Y., Domanski, K., Correa-Baena, J.-P., Nazeeruddin, M.K., Zakeeruddin, S.M., Tress, W., Abate, A., Hagfeldt, A., et al. (2016). Cesium-containing triple cation perovskite solar cells: improved stability, reproducibility and high efficiency. Energy Environ. Sci. *9*, 1989–1997.
50. Christians, J.A., Schulz, P., Tinkham, J.S., Schloemer, T.H., Harvey, S.P., Tremolet de Villers, B.J., Sellinger, A., Berry, J.J., and Luther, J.M. (2018). Tailored interfaces of unencapsulated perovskite solar cells for >1,000 hour operational stability. Nat. Energy *3*, 68–74.
51. Jacobsson, T.J., Correa-Baena, J.-P., Halvani Anaraki, E., Philippe, B., Stranks, S.D., Bouduban, M.E.F., Tress, W., Schenk, K., Teuscher, J., Moser, J.-E., et al. (2016). Unreacted PbI_2 as a Double-Edged Sword for Enhancing the Performance of Perovskite Solar Cells. J. Am. Chem. Soc. *138*, 10331–10343.
52. Park, B., Kedem, N., Kulbak, M., Lee, D.Y., Yang, W.S., Jeon, N.J., Seo, J., Kim, G., Kim, K.J., Shin, T.J., et al. (2018). Understanding how excess lead iodide precursor improves halide perovskite solar cell performance. Nat. Commun. *9*, 3301.
53. Islam, R., Chen, G., Ramesh, P., Suh, J., Fuchigami, N., Lee, D., Littau, K.A., Weiner, K., Collins, R.T., and Saraswat, K.C. (2017). Investigation of the Changes in Electronic Properties of Nickel Oxide (NiO_x) Due to UV/Ozone Treatment. ACS Appl. Mater. Interfaces *9*, 17201–17207.
54. Mason, M.G., Hung, L.S., Tang, C.W., Lee, S.T., Wong, K.W., and Wang, M. (1999). Characterization of treated indium–tin–oxide surfaces used in electroluminescent devices. J. Appl. Phys. *86*, 1688–1692.
55. Bonomo, M., Dini, D., and Marrani, A.G. (2016). Adsorption Behavior of I_3^- and I^- Ions at a Nanoporous NiO/Acetonitrile Interface Studied by X-ray Photoelectron Spectroscopy. Langmuir *32*, 11540–11550.
56. Singh, A., Chang, S.L.Y., Hocking, R.K., Bach, U., and Spiccia, L. (2013). Highly active nickel oxide water oxidation catalysts deposited from molecular complexes. Energy Environ. Sci. *6*, 579–586.
57. Wang, H.-Y., Hsu, Y.-Y., Chen, R., Chan, T.-S., Chen, H.M., and Liu, B. (2015). Ni^{3+}-Induced Formation of Active NiOOH on the Spinel Ni-Co Oxide Surface for Efficient Oxygen Evolution Reaction. Adv. Energy Mater. *5*, 1500091.
58. Electrode Potentials (2006). In Encyclopedia of Inorganic Chemistry (John Wiley & Sons, Ltd).
59. Biesinger, M.C., Payne, B.P., Grosvenor, A.P., Lau, L.W.M., Gerson, A.R., and Smart, R.S.C. (2011). Resolving surface chemical states in XPS analysis of first row transition metals, oxides and hydroxides: Cr, Mn, Fe, Co and Ni. Appl. Surf. Sci. *257*, 2717–2730.
60. Weidler, N., Schuch, J., Knaus, F., Stenner, P., Hoch, S., Maljusch, A., Schäfer, R., Kaiser, B., and Jaegermann, W. (2017). X-ray Photoelectron Spectroscopic Investigation of Plasma-Enhanced Chemical Vapor Deposited NiOx , NiOx(OH)y, and CoNiOx(OH)y: Influence of the Chemical Composition on the Catalytic Activity for the Oxygen

Evolution Reaction. J. Phys. Chem. C *121*, 6455–6463.
61. Li, Y.-F., and Selloni, A. (2014). Mosaic Texture and Double *c* -Axis Periodicity of β-NiOOH: Insights from First-Principles and Genetic Algorithm Calculations. J. Phys. Chem. Lett. *5*, 3981–3985.
62. Karsthof, R., Grundmann, M., Anton, A.M., and Kremer, F. (2019). Polaronic interacceptor hopping transport in intrinsically doped nickel oxide. Phys. Rev. B *99*, 235201.
63. Pant, N., Kulkarni, A., Yanagida, M., Shirai, Y., Miyasaka, T., and Miyano, K. (2020). Investigating the Growth of CH3NH3PbI3 Thin Films on RF-Sputtered NiOx for Inverted Planar Perovskite Solar Cells: Effect of CH3NH3+ Halide Additives versus CH3NH3+ Halide Vapor Annealing. Adv. Mater. Interfaces *7*, 1901748.
64. Onno, A., Chen, C., Koswatta, P., Boccard, M., and Holman, Z.C. (2019). Passivation, conductivity, and selectivity in solar cell contacts: Concepts and simulations based on a unified partial-resistances framework. J. Appl. Phys. *126*, 183103.
65. Stolterfoht, M., Caprioglio, P., Wolff, C.M., Márquez, J.A., Nordmann, J., Zhang, S., Rothhardt, D., Hörmann, U., Amir, Y., Redinger, A., et al. (2019). The impact of energy alignment and interfacial recombination on the internal and external open-circuit voltage of perovskite solar cells. Energy Environ. Sci. *12*, 2778–2788.
66. Bertoluzzi, L., Boyd, C.C., Rolston, N., Xu, J., Prasanna, R., O'Regan, B.C., and McGehee, M.D. (2020). Mobile Ion Concentration Measurement and Open-Access Band Diagram Simulation Platform for Halide Perovskite Solar Cells. Joule *4*, 109–127.
67. Raiford, J.A., Boyd, C.C., Palmstrom, A.F., Wolf, E.J., Fearon, B.A., Berry, J.J., McGehee, M.D., and Bent, S.F. (2019). Enhanced Nucleation of Atomic Layer Deposited Contacts Improves Operational Stability of Perovskite Solar Cells in Air. Adv. Energy Mater. *9*, 1902353.
68. Tumen-Ulzii, G., Qin, C., Klotz, D., Leyden, M.R., Wang, P., Auffray, M., Fujihara, T., Matsushima, T., Lee, J., Lee, S., et al. (2020). Detrimental Effect of Unreacted PbI $_2$ on the Long-Term Stability of Perovskite Solar Cells. Adv. Mater., 1905035.
69. Zhang, F., Xiao, C., Chen, X., Larson, B.W., Harvey, S.P., Berry, J.J., and Zhu, K. (2019). Self-Seeding Growth for Perovskite Solar Cells with Enhanced Stability. Joule *3*, 1452–1463.